

Electronic Supporting Information

A sequential logic gate-based “smart probe” for selective monitoring of Cu²⁺, Fe³⁺ and CN⁻/F⁻ *via* differential analyses

Alok Kumar Singh* and Rajamani Nagarajan*

Department of Chemistry, University of Delhi, Delhi-110 007, India.

***E-mail: aloksinghchemistry@gmail.com**

Material and Methods: Most of the salts for sensing experiment were purchased from BDH chemicals Ltd, Sigma Adrich and used as received. $\text{RuCl}_3 \cdot x\text{H}_2\text{O}$ was purchased from Sigma Adrich and store in N_2 atmosphere. 2, 5-Dichloro-3, 6-dihydroxy-1, 4-benzoquinone (Chloranilic acid) and 2, 2'-bipyridine were purchased from Alfa Aesar and used as received. $\text{DMSO-}d_6$ was purchased from Sigma Aldrich and stored under freezer. Acetonitrile (HPLC grade) and ethanol were purchased from Merck and distilled using reported methods.^{S1} Double distilled water was used for the experiment. UV-vis-NIR spectra were recorded using an analytikjena SPECORD 250 with a quartz cuvette (path length = 1 cm, volume = 3 ml). $^1\text{H-NMR}$ spectrum was recorded on Jeol JNMECX 400p spectrometer at room temperature using $\text{DMSO-}d_6$. All chemical shifts (δ) were recorded in ppm with reference to TMS and coupling constant (J) in Hz. FTIR spectra were recorded on Perkin-Elmer spectrophotometer in range 400-4000 cm^{-1} using KBr as a medium. The pH of the solution was fixed with EUTECH Instruments pH 510, calibrated with buffer solution of pH 4.00 and 9.00 before each measurement. The pH of test solution was adjusted with $\sim 10^{-3}$ M HCl and NaOH solution in distilled H_2O . X-ray diffraction data for **1** was collected on the Oxford Diffractometer at room temperature equipped with a CCD detector using graphite-monochromated Mo- $K\alpha$ radiation ($\lambda = 0.71073 \text{ \AA}$). The optical probe **1** was synthesised following only some modification in the reported synthetic method by Kawata and co-workers.^{S2}

Synthesis of optical probe (1). $\text{Ru}(\text{bpy})_2\text{Cl}_2 \cdot 2\text{H}_2\text{O}$ (80.3 mg, 0.15 mmol) was dissolved in $\text{N,N}'$ -dimethylformamide (DMF) (30 mL). Chloranilic acid (32.29 mg, 0.15 mmol) and sodium hydroxide (12.39 mg, 0.31 mmol) in ethanol (20 mL) were added dropwise to the solution under a N_2 atmosphere with constant stirring. The reaction-mixture was refluxed with stirring for 4 h, and a black precipitate was formed, collected by vacuum filtration. The residue was washed with water followed by diethyl ether and dried under vacuum. Yield: 49.57 mg (52%). $^1\text{H-NMR}$ (400 MHz, $\text{DMSO-}d_6$): δ (ppm) = 8.78 (d, 2H, $J = 8.4 \text{ Hz}$), 8.65 (d, 2H, $J = 8.8 \text{ Hz}$), 8.57 (d, 2H, $J = 5.2 \text{ Hz}$), 8.17 (td, 2H, $J = 1.2 \text{ Hz}$, $J = 1.2 \text{ Hz}$, $J = 1.2 \text{ Hz}$), 7.88-7.79 (m, 4H), 7.57 (d, 2H, $J = 5.2 \text{ Hz}$), 7.24 (td, 2H, $J = 1.6 \text{ Hz}$, $J = 1.6 \text{ Hz}$, $J = 1.6 \text{ Hz}$); FTIR: ν (cm^{-1}) = 1606, 1518, 1476, 1419, 1357, 1307, 1231, 1010, 833, 756; ESI-MS (calculated for $\text{C}_{28}\text{H}_{19}\text{Cl}_2\text{N}_5\text{O}_4\text{Ru}$): 620.80 [$\text{M-CH}_3\text{CN}$]; UV-vis (10^{-5} M, $\text{CH}_3\text{CN/DMF}$, 7:3, v/v): $\lambda_{\text{max}} = 524 \text{ nm}$ ($\epsilon = 15,634 \text{ M}^{-1} \text{ cm}^{-1}$).

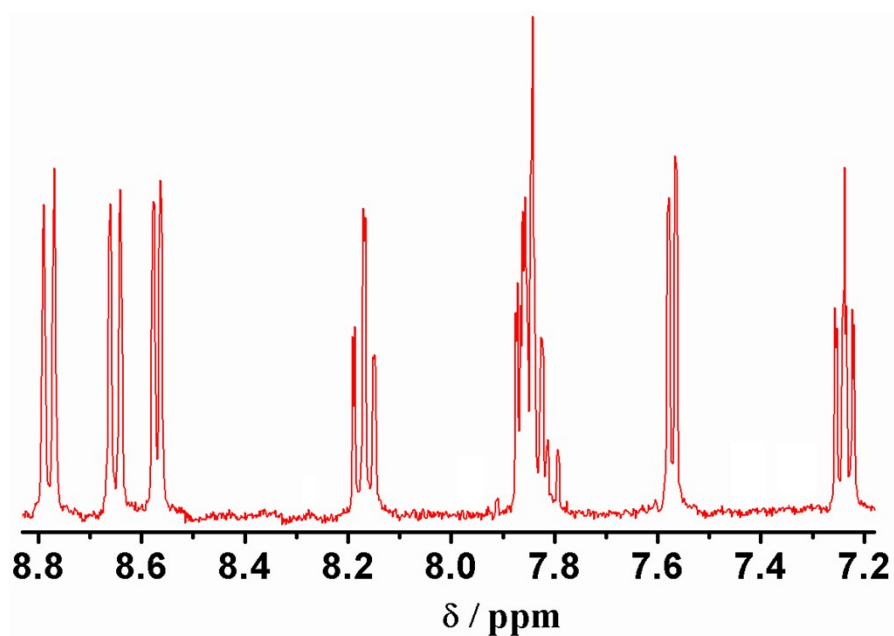


Figure S1: ¹H-NMR spectrum of **1** in DMSO-*d*₆ at room temperature.

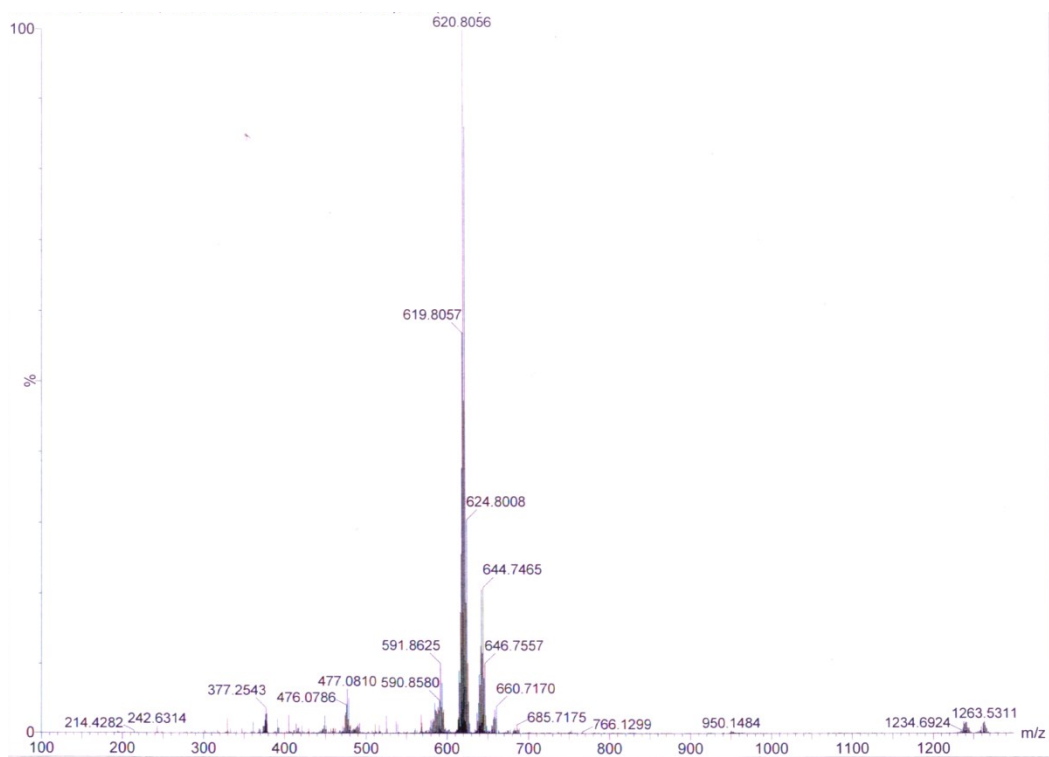


Figure S2: ESI-MS spectrum of **1**.

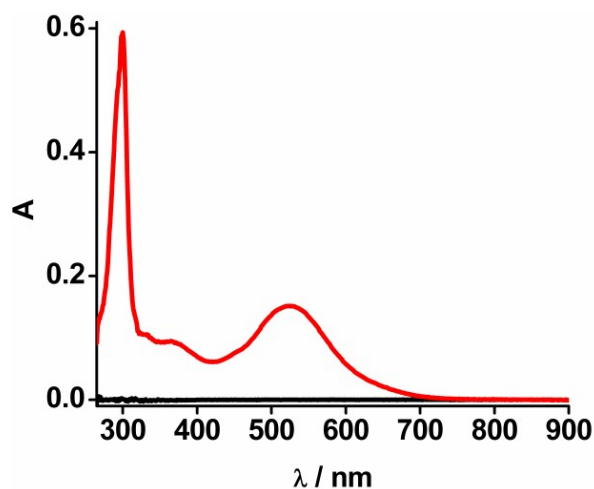


Figure S3: UV-vis spectrum of **1** (10^{-5} M, CH₃CN/DMF, 7:3, v/v) at room temperature.

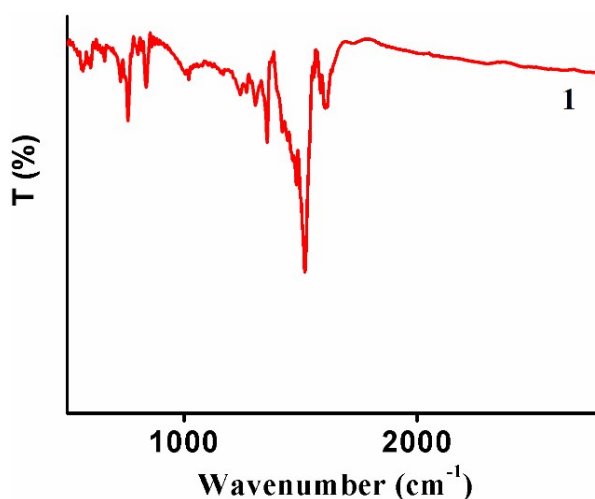


Figure S4: FTIR spectrum of **1**.

Crystallographic Information:

X-ray Crystal structure determination: Suitable crystal for structure determination was obtained by slow evaporation of acetonitrile solution of **1** for one/two week at room temperature. The structure was solved using direct and Fourier methods and refined by full-matrix least squares based on F^2 using WINGX software, which operated SHELX-97 software. The non-H atoms were refined anisotropically. The final least-squares refinement [$I > 2\sigma(I)$] converged to reasonably good R values, $R_1 = 0.0823$, $wR_2 = 0.2449$ for **1**. The goodness of fit for **1** is 1.219. The maximum and minimum peaks on the final difference Fourier map corresponding to 2.352 and $-1.061 \text{e}\text{\AA}^{-3}$ (**1**). Complex **1** crystallized in the triclinic form with space group $P-1$.

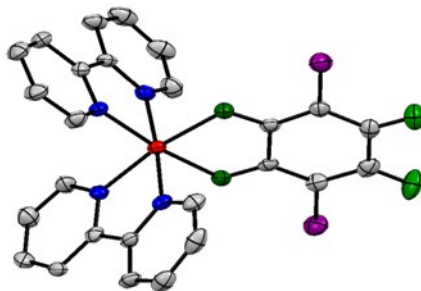


Figure S5: ORTEP representation of **1** (thermal ellipsoids are drawn at 30% probability level). H atoms and acetonitrile are omitted for clarity.

Summary of crystal data of 1:

Empirical formula	$C_{28}H_{19}Cl_2N_5O_4Ru$
Formula weight	661.45
Temperature	293(2) K
Wavelength	0.71073 Å
Crystal system	Triclinic
Space group	$P - 1$
Unit cell dimensions	$a = 9.608(5) \text{ \AA}$ $\alpha = 97.457(5)^\circ$. $b = 9.713(5) \text{ \AA}$ $\beta = 99.221(5)^\circ$. $c = 14.956(5) \text{ \AA}$ $\gamma = 104.685(5)^\circ$.
Volume	$1311.3(11) \text{ \AA}^3$
Z	2
Density (calculated)	1.675 Mg/m^3
Absorption coefficient	0.848 mm^{-1}
F (000)	664
Theta range	2.805 to 24.999°
Index ranges	$-11 \leq h \leq 11$, $-11 \leq k \leq 11$, $-17 \leq l \leq 17$
Reflections collected	16315
Independent reflections	4608 [R(int) = 0.0666]
Completeness to theta = 25.00°	99.8%
Refinement method	Full-matrix least-squares on F^2
Goodness-of-fit on F^2	1.219
Final R indices [$I > 2 \text{ sigma}(I)$]	$R_1 = 0.0823$, $wR_2 = 0.2449$
R indices (all data)	$R_1 = 0.0942$, $wR_2 = 0.2526$
Largest diff. peak and hole	2.352 and $-1.061 \text{ e} \text{ \AA}^{-3}$

Preparation of ppm-level solutions. A stock solution of 1000 ppm of various salts of $Cd(NO_3)_2 \cdot 4H_2O$, $AgNO_3$, $Hg(NO_3)_2 \cdot H_2O$, $FeCl_3$, $LiNO_3$, $CaCl_2$, $Co(NO_3)_2 \cdot 6H_2O$, KNO_3 , $FeSO_4 \cdot 7H_2O$, $Pb(NO_3)_2$, $MgSO_4 \cdot 7H_2O$, $MnCl_2 \cdot 4H_2O$, $Ni(NO_3)_2 \cdot 6H_2O$, $Cr(NO_3)_3 \cdot 9H_2O$, $ZnSO_4 \cdot 7H_2O$, $Cu(NO_3)_2 \cdot 3H_2O$, KCN , KF , KNO_2 , $KSCN$, NH_4PF_6 , $NaClO_4$, KI , KBr and

KCl were made by dissolving 10 mg of each salts in 10 ml of suitable solvents, water for aqueous medium and mixture of dry solvents *i.e.*, acetonitrile/ethanol/DMSO for non-aqueous medium. Moreover, the stock solution was diluted to 1 ppm by taking 5 μ l volume of stock solution (1000 ppm) and making up it in solution of 1 upto 5 ml. The solution was used for analyses. For proof-of-concept experiments, pool and tap water samples were collected and filtered before preparing stock solution (1000 ppm) of Cu²⁺ and Fe³⁺.

Detection procedure of ppm-levels of Cu²⁺ and Fe³⁺: A 5 ml solution of **1** (10⁻⁵ M, CH₃CN/DMF, 7:3, v/v) was treated with 5 μ l stock solution (1000 ppm) of Cu²⁺/Fe³⁺ (1.0 ppm in solution of **1**), mixed well within seconds. The resulting solution was used for recording absorbance spectra at room temperature. The similar methodology was executed for higher concentrations of Cu²⁺ and Fe³⁺.

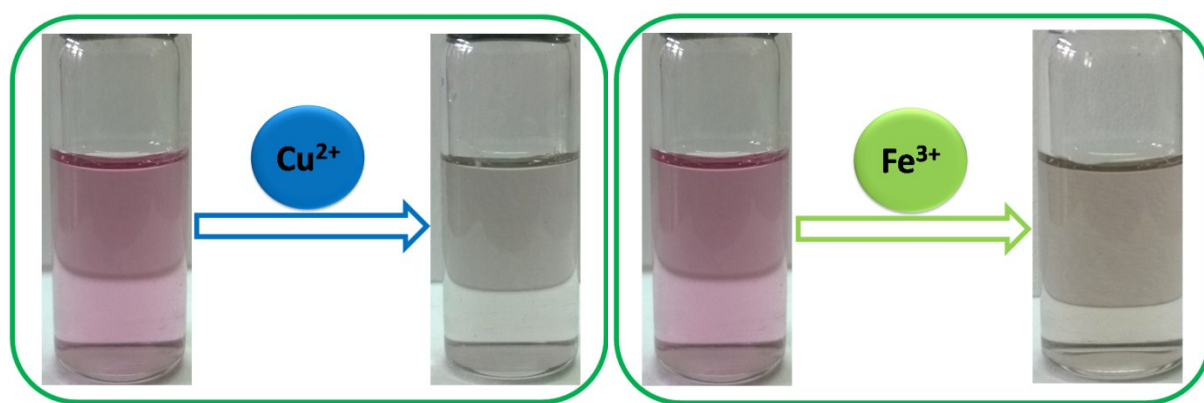


Figure S6: Colorimetric changes in **1** (10⁻⁵ M, CH₃CN/DMF, 7:3, v/v) upon addition of 15 ppm of Cu²⁺ and 20 ppm of Fe³⁺ in water.

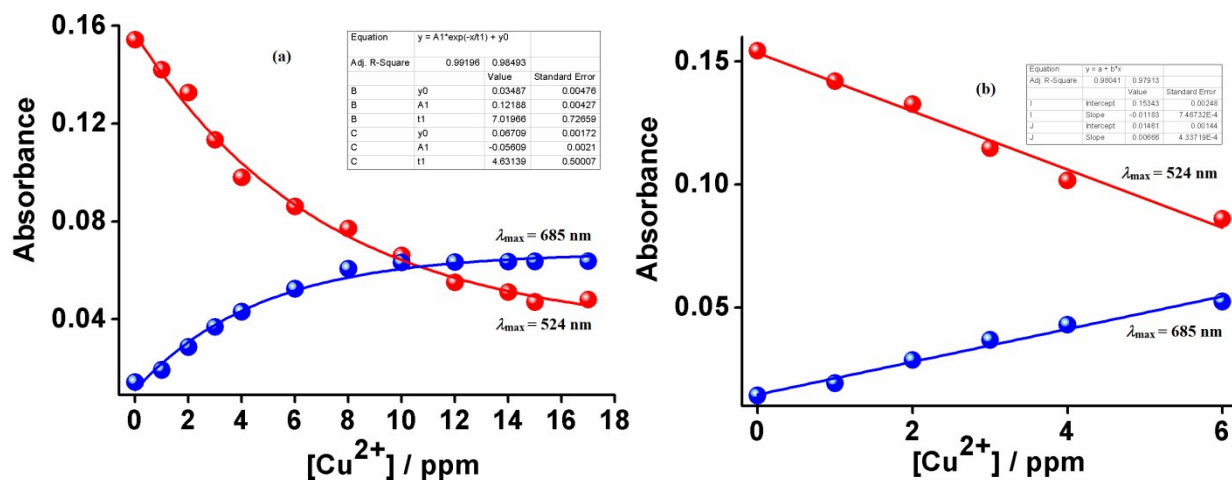


Figure S7: (a) Plot of absorbance at $\lambda_{\max} = 524$ nm (red balls, $R^2 = 0.99$) and $\lambda_{\max} = 685$ nm (blue balls, $R^2 = 0.98$) as a function of ppm concentrations of Cu^{2+} in H_2O . (b) Plot of absorbance at $\lambda_{\max} = 524$ nm (red balls, $R^2 = 0.98$) and $\lambda_{\max} = 685$ nm (blue balls, $R^2 = 0.97$) as a function of lower ppm concentrations of Cu^{2+} in H_2O .

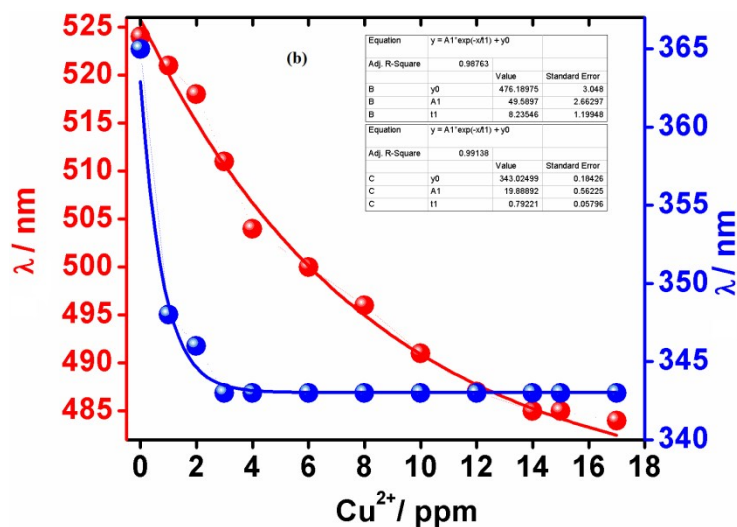


Figure S8: Change in wavelength as a function of ppm concentrations of Cu^{2+} in H_2O for MLCT band (red balls, $R^2 = 0.98$) and new band (blue balls, $R^2 = 0.99$).

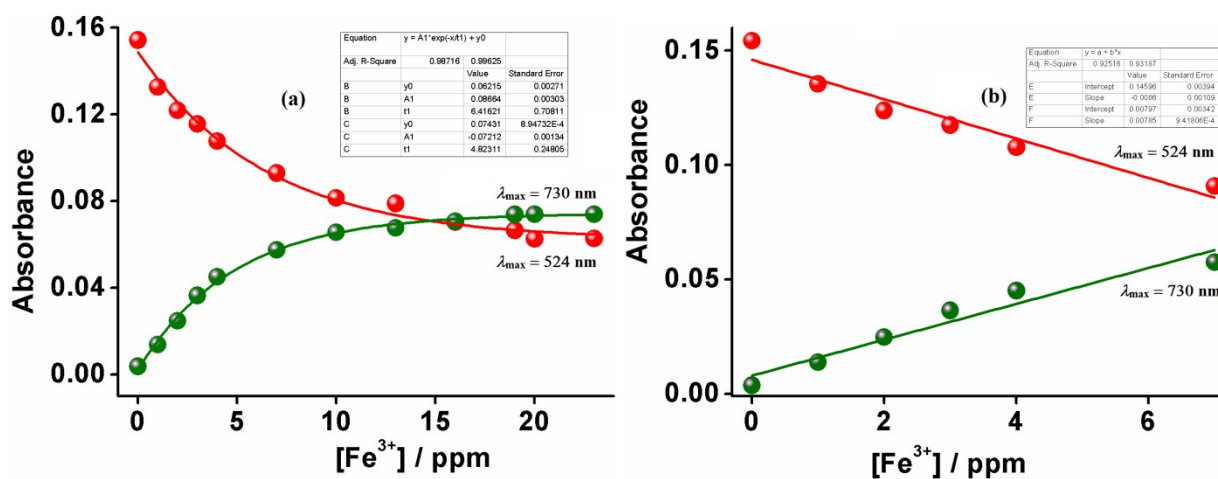


Figure S9: (a) Plot of absorbance at $\lambda_{\max} = 524$ nm (red balls, $R^2 = 0.98$) and $\lambda_{\max} = 730$ nm (olive balls, $R^2 = 0.99$) as a function of ppm concentrations of Fe^{3+} in H_2O . (b) Plot of absorbance at $\lambda_{\max} = 524$ nm (red balls, $R^2 = 0.92$) and $\lambda_{\max} = 730$ nm (olive balls, $R^2 = 0.93$) as a function of lower ppm concentrations of Fe^{3+} in H_2O .

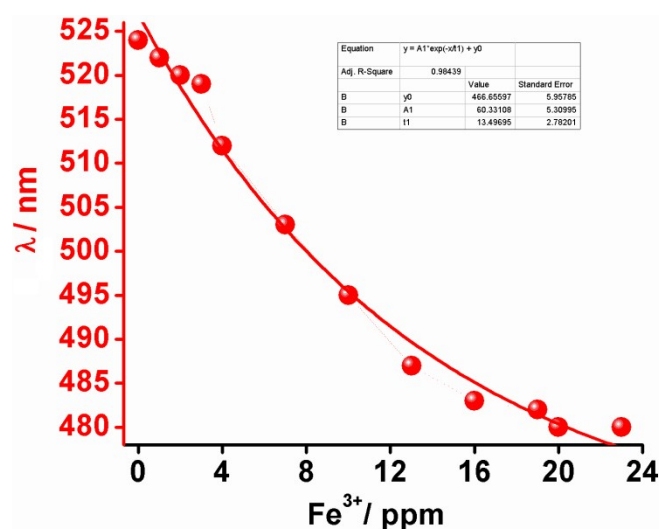


Figure S10: Change in wavelength as a function of ppm concentrations of Fe^{3+} in H_2O for MLCT band (red balls, $R^2 = 0.98$).

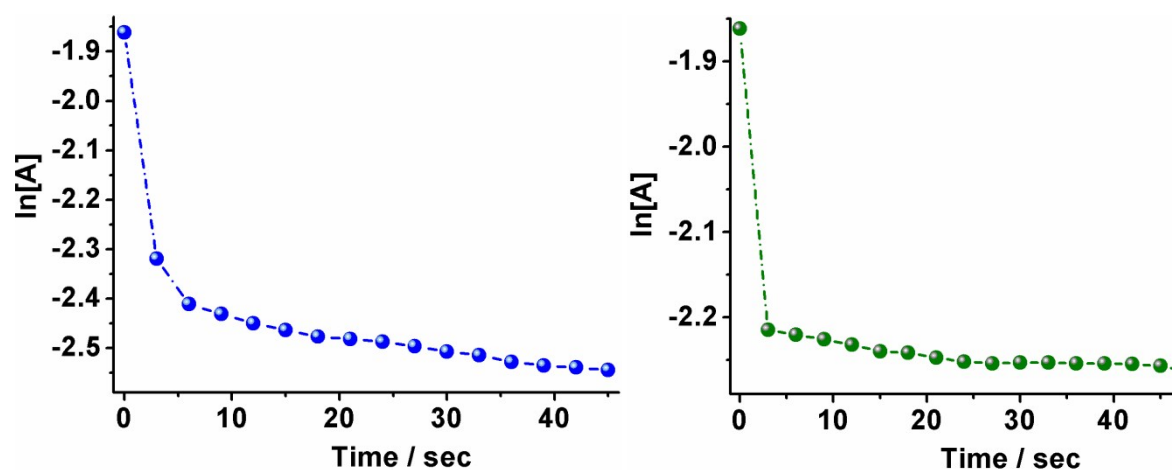


Figure S11: Representative plot between change in absorbance ($\ln[A]$) of **1** (10^{-5} M, $\text{CH}_3\text{CN}/\text{DMF}$, 7:3, v/v) vs. time (in seconds) at MLCT band, $\lambda_{\text{max}} = 524$ nm upon addition of 15 ppm of Cu^{2+} (blue balls) and 20 ppm of Fe^{3+} (olive balls) in H_2O .

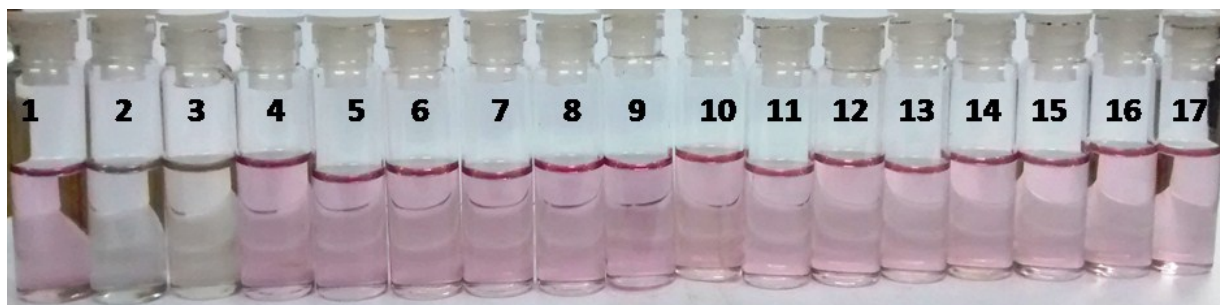


Figure S12: Visual colour changes in the solution of **1** (10^{-5} M, $\text{CH}_3\text{CN}/\text{DMF}$, 7:3, v/v) on addition of 20 ppm of different cations in H_2O . 1 = Complex, 2 = 1+ Cu^{2+} , 3 = 1+ Fe^{3+} , 4 = 1+ Hg^{2+} , 5 = 1+ Li^+ , 6 = 1+ Mg^{2+} , 7 = 1+ Co^{2+} , 8 = 1+ K^+ , 9 = 1+ Fe^{2+} , 10 = 1+ Pb^{2+} , 11 = 1+ Ca^{2+} , 12 = 1+ Mn^{2+} , 13 = 1+ Ni^{2+} , 14 = 1+ Cr^{3+} , 15 = 1+ Zn^{2+} , 16 = 1+ Cd^{2+} , 17 = 1+ Ag^+ .

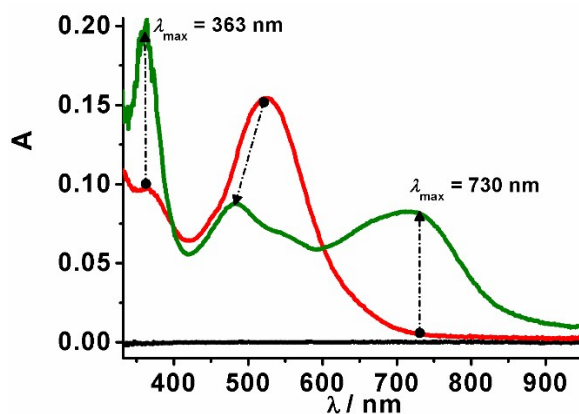


Figure S13: Absorbance changes of **1** (10^{-5} M, $\text{CH}_3\text{CN}/\text{DMF}$, 7:3 v/v) (red) upon addition of inputs 15 ppm of Cu^{2+} and 20 ppm of Fe^{3+} in H_2O .

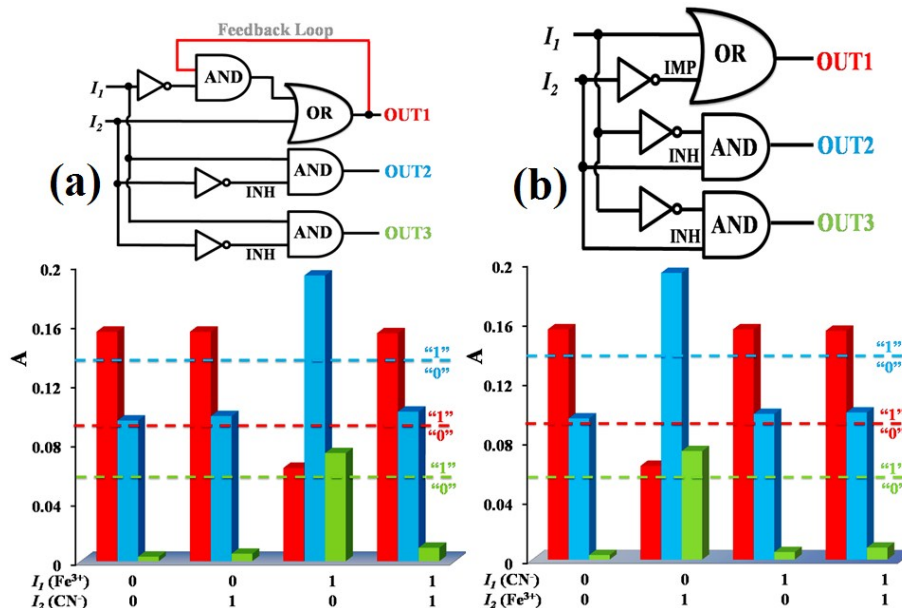


Figure S14: Absorbance outputs of **1** at $\lambda_{\max} = 524 \text{ nm}$ (OUT1, red bars), $\lambda_{\max} = 363 \text{ nm}$ (OUT2, light blue bars) and $\lambda_{\max} = 730 \text{ nm}$ (OUT3, light green bars) in the presence of chemical inputs *viz.* (a) I_1 (Fe^{3+}) and I_2 (CN^-) and the corresponding two-input sequential logic circuit. (b) I_1 (CN^-) and I_2 (Fe^{3+}) and the corresponding two-input combinatorial logic circuit. Dotted lines represent the threshold level of absorbance outputs. Threshold level = 0.09 for OUT1, 0.14 for OUT2 and 0.065 for OUT3. The output above the threshold level is read as “1” otherwise “0”.

Input		Output	
I_1 Fe^{3+}	I_2 Cu^{2+}	OUT1 $\lambda_{\max} = 685 \text{ nm}$	OUT2 $\lambda_{\max} = 730 \text{ nm}$
0	0	0	0
0	1	1	0
1	0	0	1
1	1	0	1

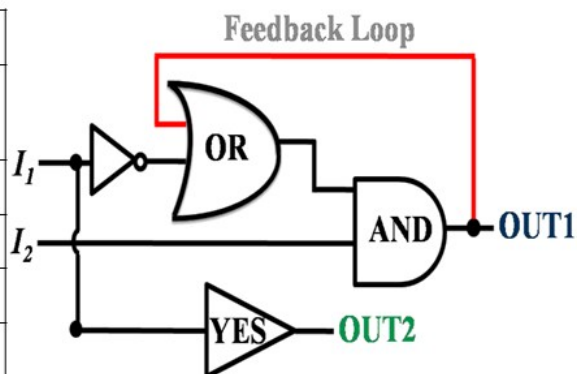


Figure S15: Truth table for sequential logic operations with two inputs based on compound **1**. Note: **1** could be viewed as a gate and Fe^{3+} and Cu^{2+} could act as two inputs. The absence and presence of these inputs was considered as 0 and 1, respectively. Threshold level =

0.055 for OUT1 and 0.065 for OUT2. The output above the threshold level is read as “1” otherwise “0”.

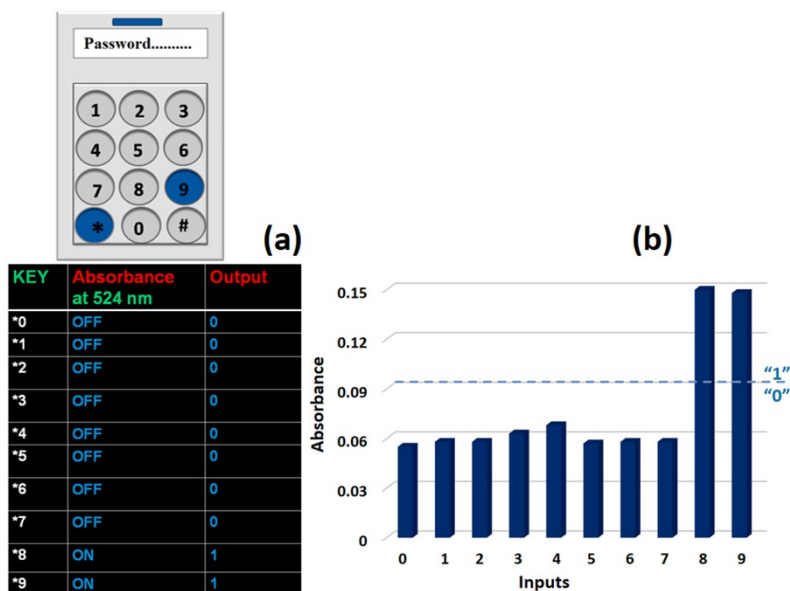


Figure S16: (a) A molecular keypad lock with absorbance output at MLCT band, $\lambda_{\max} = 524$ nm (Threshold level = 0.09). When the correct password “*8” (* = Cu^{2+} , 8 = CN^-) or “*9” (* = Cu^{2+} , 9 = F^-) is entered absorbance channel is turned on. The table shows the output in the absorbance channel and the overall output in response to the different input combinations; (b) Representative bar chart showing absorbance change at $\lambda_{\max} = 524$ nm upon addition of various inputs (20 ppm of anions in H_2O) in the solution of **1**- Cu^{2+} (15 ppm of Cu^{2+} in 10^{-5} M of **1**, blue bars) (* = Cu^{2+} , # = Fe^{3+} , 0 = NO_3^- , 1 = SCN^- , 2 = Br^- , 3 = PF_6^- , 4 = ClO_4^- , 5 = NO_2^- , 6 = I^- , 7 = Cl^- , 8 = CN^- , 9 = F^-). Dotted lines represent the threshold level of absorbance outputs. The absorbance greater than the threshold values are allocated as “1” and absorbance smaller than the threshold values are allocated as “0”.

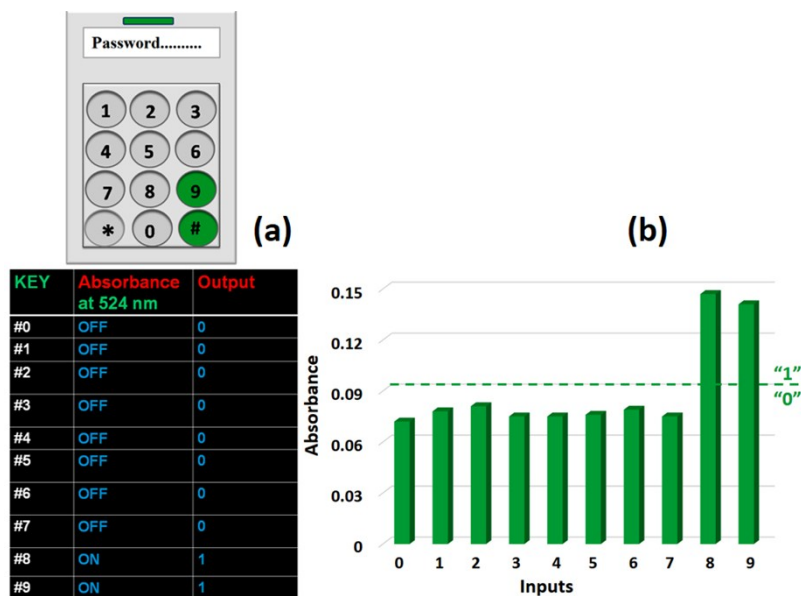


Figure S17: A molecular keypad lock with absorbance output at MLCT band, $\lambda_{\max} = 524$ nm (Threshold level = 0.09). When the correct password “#8” (# = Fe^{3+} , 8 = F^-) or “#9” (# = Fe^{3+} , 9 = CN^-) is entered absorbance channel is turned on. The table shows the output in the absorbance channel and the overall output in response to the different input combinations; (b) Representative bar chart showing absorbance change at $\lambda_{\max} = 524$ nm upon addition of various inputs (20 ppm of anions in H_2O) in the solution of **1**- Fe^{3+} (20 ppm of Fe^{3+} in 10^{-5} M of **1**, olive bars) (* = Cu^{2+} , # = Fe^{3+} , 0 = NO_3^- , 1 = SCN^- , 2 = Br^- , 3 = PF_6^- , 4 = ClO_4^- , 5 = NO_2^- , 6 = I^- , 7 = Cl^- , 8 = CN^- , 9 = F^-). Dotted lines represent the threshold level of absorbance outputs. The absorbance greater than the threshold values are allocated as “1” and absorbance smaller than the threshold values are allocated as “0”.

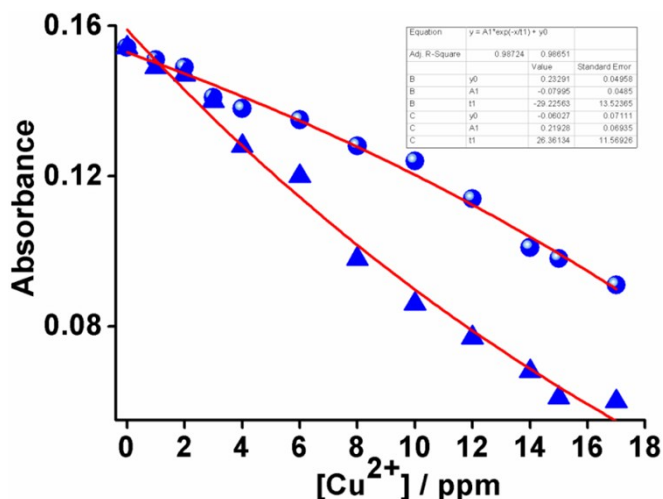


Figure S18: Proof-of-concept experiments with probe **1** (at $\lambda_{\max} = 524$ nm, MLCT band) for determining Cu^{2+} in pool (blue balls, $R^2 = 0.98$) and tap water (blue triangles, $R^2 = 0.98$) solutions.

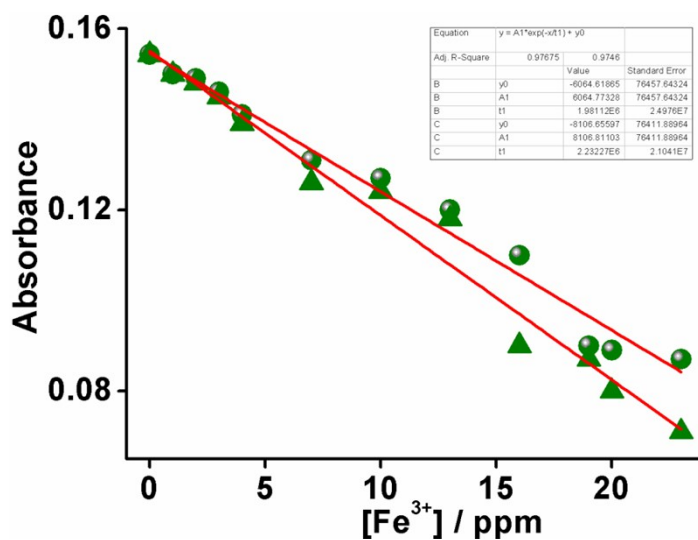


Figure S19: Proof-of-concept experiments with probe **1** (at $\lambda_{\max} = 524$ nm, MLCT band) for determining Fe^{3+} in pool (olive balls, $R^2 = 0.97$) and tap water (olive triangles, $R^2 = 0.97$) solutions.

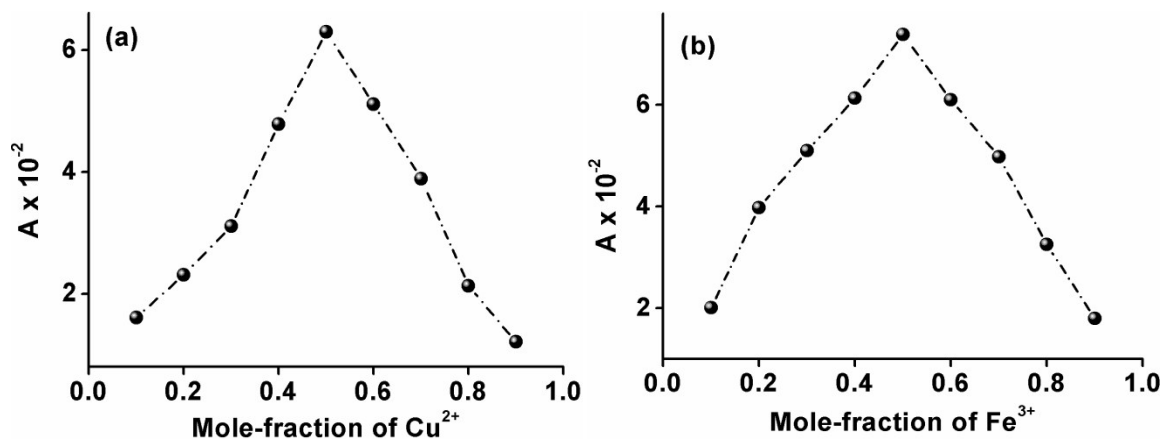


Figure S20: Job's plot for varying mole-fraction of (a) Cu^{2+} at $\lambda_{\text{max}} = 685 \text{ nm}$ and (b) Fe^{3+} at $\lambda_{\text{max}} = 730 \text{ nm}$ in **1** (10^{-5} M).

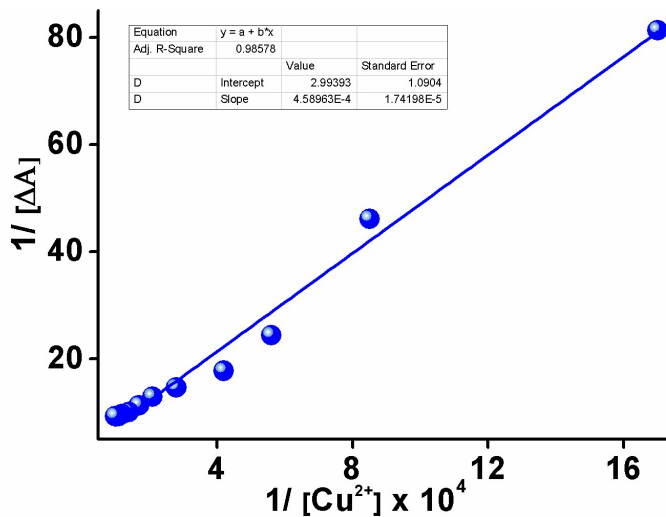


Figure S21: Benesi-Hildebrand plot showing reciprocal of change in absorption of **1** vs. reciprocal of concentration of Cu^{2+} ($R^2 = 0.98$) at $\lambda_{\text{max}} = 524 \text{ nm}$ (MLCT band).

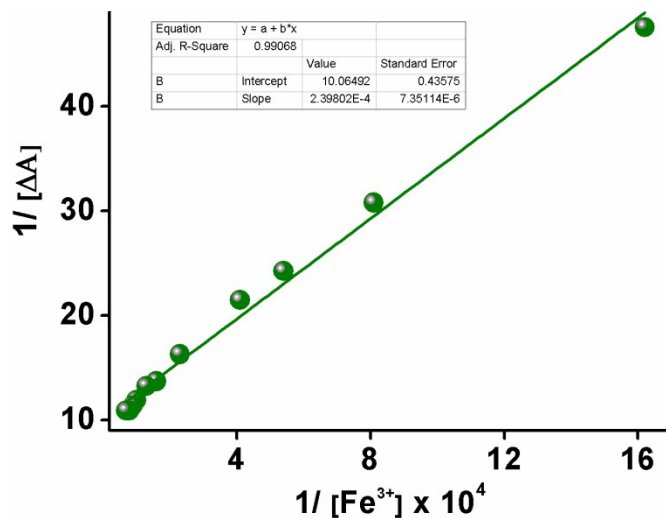


Figure S22: Benesi-Hildebrand plot showing reciprocal of change in absorption of **1** vs. reciprocal of concentration of Fe^{3+} ($R^2 = 0.99$) at $\lambda_{\text{max}} = 524 \text{ nm}$ (MLCT band).

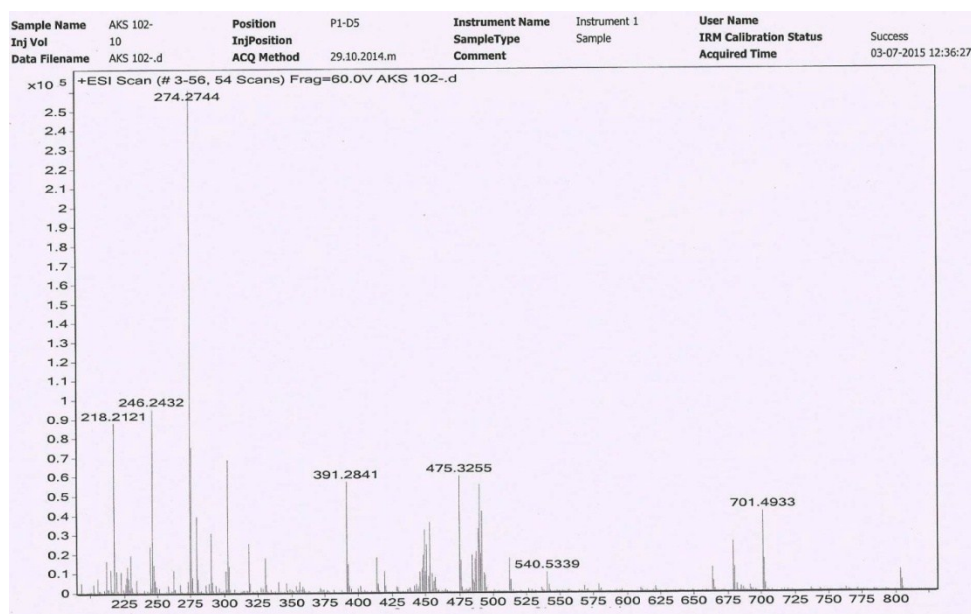


Figure S23: ESI-MS spectrum of **1-Cu²⁺** in CH_3CN at room temperature (peak at $m/z = 274.2744$ corresponds to fragment $[\mathbf{1}.\text{CH}_3\text{CN}-\text{Cl}+\text{Cu}(\text{CH}_3\text{CN})_2.3\text{H}_2\text{O}]^{3+}$; $m/z = 391.2841$ corresponds to fragment $[\mathbf{1}.\text{CH}_3\text{CN}+\text{Cu}(\text{CH}_3\text{CN}).\text{H}_2\text{O}]^{2+}$; $m/z = 475.3255$ corresponds to fragment $[\mathbf{1}.\text{CH}_3\text{CN}+\text{Cu}(\text{CH}_3\text{CN})_2.2\text{NO}_3.\text{H}_2\text{O}]^{2+}$; $m/z = 701.4933$ corresponds to fragment $[\mathbf{1}.2\text{CH}_3\text{CN}]$).

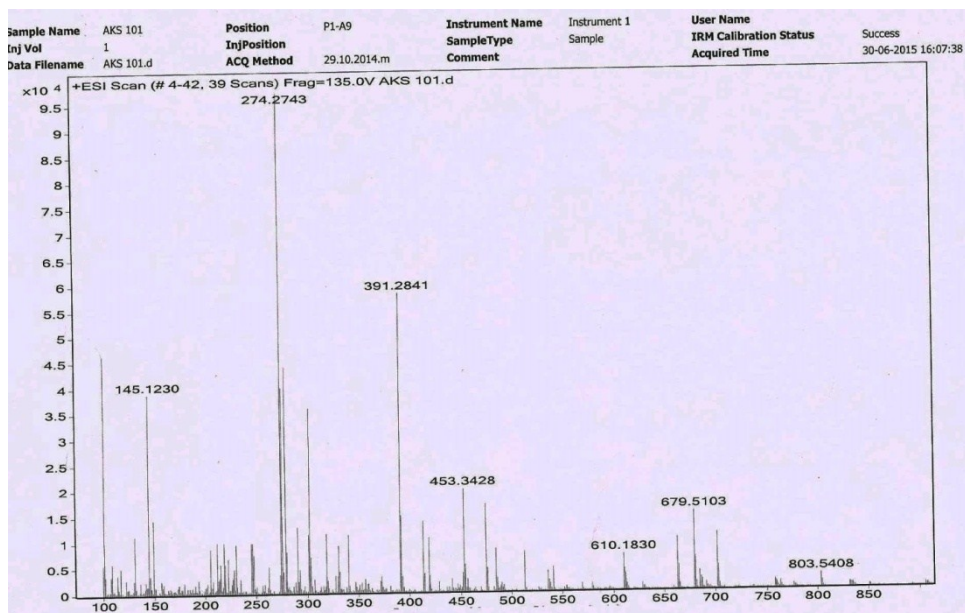
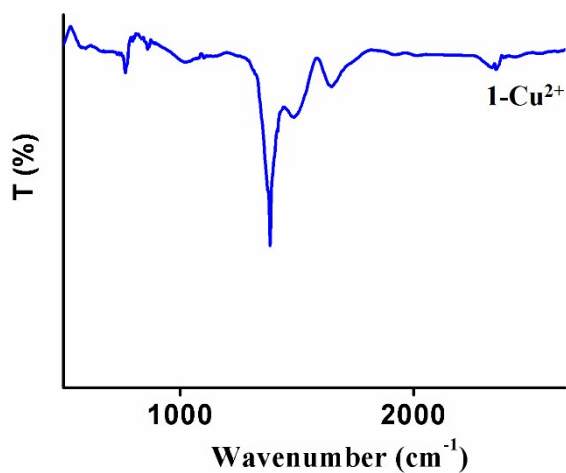


Figure S24: ESI-MS spectrum of **1-Fe³⁺** in CH₃CN at room temperature (peak at $m/z = 274.2743$ corresponds to fragment $[1.CH_3CN+Fe(H_2O)_6]^{3+}$; $m/z = 803.5408$ corresponds to fragment $[1+FeCl_3+Na^+]$; $m/z = 391.2841$ corresponds to fragment $[1+Fe(H_2O)_4.Cl]^{2+}$; $m/z = 453.3428$ corresponds to fragment $[1.CH_3CN+Fe(H_2O)_4.Cl.2CH_3CN]^{2+}$; $m/z = 679.5103$ corresponds to fragment $[1.CH_3CN.H_2O]$).



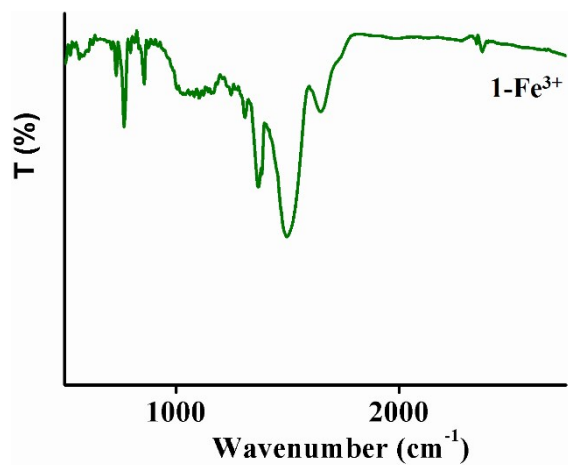


Figure S25: FTIR spectra of **1-Cu²⁺** and **1-Fe³⁺** at room temperature.

References:

S1. D. D. Perrin and W. L. F. Armarego, *Purification of Laboratory Chemicals*, 3. Aufl., Oxford. Pergamon Press, 1988.

S2. R. Ishikawa, M. K. Kabir, K. Adachi, K. Nozaki and S. Kawata, *Chem. Lett.*, 2007, **36**, 1116.